Catena 160 (2018) 201–211

Contents lists available at ScienceDirect

Catena

journal homepage: www.elsevier.com/locate/catena

Improving sediment load estimations: The case of the Yarlung Zangbo River (the upper Brahmaputra, Tibet Plateau)

Chen Zeng[a,b], Fan Zhang[a,b,c,*], Xixi Lu[d], Guanxing Wang[a,b,e], Tongliang Gong[f]

[a] Key Laboratory of Tibetan Environment Changes and Land Surface Processes, Institute of Tibetan Plateau Research, Chinese Academy of Sciences, Beijing 100101, China
[b] Key Laboratory of Alpine Ecology and Biodiversity, Institute of Tibetan Plateau Research, Chinese Academy of Sciences, Beijing 100101, China
[c] CAS Center for Excellence in Tibetan Plateau Earth Sciences, Beijing 100101, China
[d] Department of Geography, National University of Singapore, Singapore
[e] University of Chinese Academy of Sciences, Beijing 100049, China
[f] Hydrological Bureau in the Tibet Autonomous Region, Lhasa 850000, China

ARTICLE INFO

Keywords:
Suspended sediment concentration
Suspended sediment load
Sediment rating curve
Flood rank
The Tibetan plateau

ABSTRACT

Suspended sediment load of a river represents integrated results of soil erosion, landform change and ecosystem variation occurring within the river basin. Accurate estimation of suspended sediment load is helpful for distinguishing the impact of natural and anthropogenic factors on earth system processes within river basin under global climate change. Suspended sediment load, with long-term in-situ observation limited by harsh conditions, can be estimated by sediment rating curves and various subdivision methods with suspended sediment concentration and discharge data of low-frequency. New sediment rating curve subdivision methods based on flood ranks and suspended sediment concentration stages were proposed in this study. The flood ranks subdivision method, which defined a flood to begin when discharge exceeded the critical discharge value (rank1) or the previous peak flow (rank2 and the later), and end when fluctuating discharge reached the peak flow of current flood again (which is the beginning of next flood) or lowered to the critical discharge value (the last rank), was suitable for application in the basin where sediments were mainly transported and exhausted in early events. The suspended sediment concentration stages subdivision method, i.e. the rising and falling limbs of suspended sediment concentration separated by peak dates estimated based on accumulated precipitation, was suitable for application in the basin where soil erosion was closely related to precipitation. Compared to the traditional sediment rating curve, and seasonal, discharge classes and discharge stages subdivision methods, these newly proposed methods can improve suspended sediment concentration and subsequently suspended sediment load estimation in the middle reach of the Yarlung Zangbo River with higher coefficients of determination and Nash-Sutcliffe efficiency coefficients and lower bias and root-mean-square errors. Moreover, combination of the two separately developed methods presented further improved estimation. The newly proposed sediment rating curve subdivision methods could be helpful for suspended sediment load estimation and therefore are useful for water resource management within river basins.

1. Introduction

Suspended sediment load (*SSL*) of a river represents an integrated measure of erosion, sediment transport and deposition processes occurring within the river basin over a specified time period (Delmas et al., 2011). Transport of sediment from rivers to the ocean is one of the main pathways in the global geochemical cycle, and plays an important role in transferring sediment and associated material, including organic carbon and heavy metals (Schäfer et al., 2002; Lal, 2003; Audry et al., 2004). Change in *SSL* can induce variations of downstream channel erosion and delta sedimentation in many fluvial systems (Lu and Siew, 2006; Milliman and Farnsworth, 2011; Dai and Liu, 2013). With the increased interest in global climate and environmental change, quantitative analysis of river *SSL* is an important tool for assessing earth system processes, and for understanding the impacts of natural and anthropogenic disturbances on geomorphic processes within river basins (Vörösmarty et al., 2003; Walling and Fang, 2003).

Long term observation of *SSL*, which is estimated from water discharge (*Q*) and suspended sediment concentration (*SSC*) in rivers, is important for river basin management (Asselman, 2000). Although discharge can be measured automatically and continuously, or near-continuously (Horowitz, 2003; Delmas et al., 2011), the availability and

* Corresponding author at: Institute of Tibetan Plateau Research, CAS, China.
E-mail address: zhangfan@itpcas.ac.cn (F. Zhang).

http://dx.doi.org/10.1016/j.catena.2017.09.023
Received 16 December 2016; Received in revised form 25 September 2017; Accepted 25 September 2017
Available online 29 September 2017
0341-8162/

reliability of *SSL* data are limited and usually with a coarse resolution because *SSC* data are mainly obtained from infrequent sampling due to the high cost of operation and maintenance of samplers. Therefore, low-frequency *SSC* data is a limiting factor in sediment dynamics research.

For rivers with harsh observation conditions, high-frequency *SSC* data are usually insufficient. Therefore, various approaches have been developed for estimating *SSC*, including averaging estimators, ratio estimators and regression methods (Quilbé et al., 2006). For averaging estimators, only the available *Q* and *SSC* data were used to estimate mean *SSL* (Walling and Webb, 1988). For ratio estimators, covariance between *Q* and *SSC* was taken into account (Beale, 1962). For regression methods, empirical relationships were established between the *Q* and *SSC*. Among the regression methods, sediment rating curve (SRC), which presents the relation between *Q* and *SSC* by linear, power, and polynomial functions, etc., have been widely applied in previous studies (Walling, 1974; Wood, 1977; Preston et al., 1989; Asselman, 2000; Vericat and Batalla, 2006; Ali and Boer, 2007; Delmas et al., 2011; Tananaev, 2013; Mei et al., 2015). The most common expression of SRC is a power function (Walling, 1974), described as:

$$SSC = aQ^b \quad (1)$$

where *SSC* is suspended sediment concentration (kg/m^3), *Q* is water discharge (m^3/s), and *a* and *b* are regression coefficients. In recent studies, the two regression coefficients were typically estimated by nonlinear least squares regression, the best fitting procedure recommended by Asselman (2000). However, the log-transformation of *Q* and *SSC* data, prior to the analysis of SRC in the power relation, could substantially underestimate actual *SSC* (Horowitz, 2003). Although the regression coefficients *a* and *b* have no physical meaning, they have often been described as index of the soil erodibility and river flow erosivity, respectively (Peters-Kümmerly, 1973; Morgan, 1995).

The traditional SRCs were based on the hypothesis that a general relation exists between *Q* and *SSC*. In reality, this relation is usually not homogeneous due to varying river basin conditions, including seasonal effect, flow dynamics, sediment availability, and anthropogenic activities (Horowitz, 2003). As a consequence, some traditional SRCs were further developed by subdividing the *Q* and *SSC* data into different groups. For example, some SRCs were grouped by seasonal classes (Walling, 1977), by discharge classes (e.g. low, normal and high flow) (Preston et al., 1989; De Girolamo et al., 2015), by discharge stages based on rising and falling limbs (Delmas et al., 2011), or by pre −/post- periods of construction of dams (Kesel, 1989). These subdivision methods were verified to improve estimation results of *SSC* and *SSL* in many large rivers around the world, such as the Amazon River (Devol et al., 1986), the Mississippi River (Sivakumar and Chen, 2006), the Danube River (Mladenovic et al., 2013; Tóth and Bódis, 2015), the Rhine River (Asselman, 2000), the Nile River (Abdelazim et al., 2007), the Indus River (Ali and Boer, 2007), the Ganges River (Abbas and Subramanian, 1984), the Yangtze River (Xu et al., 2005) and the Yellow River (Shi, 2015).

The aims of this paper are to evaluate and improve SRCs for estimating *SSC* and, subsequently, *SSL* based on analysis of *Q* and *SSC* variability in the middle reach of the Yarlung Zangbo River over a period of three years. The purpose is to develop better SRC subdivision methods that are useful for water resource managers to evaluate *SSL*.

2. Material and methods

2.1. Study region

The Yarlung Zangbo River (hereafter YZR) (80°12′-97°38′E, 27°26′-28°54′N), originates from the Jiemayangzong Glacier at an elevation of 5590 m on the northern slope of the Himalayas, and flows from west to east across the southern part of the Tibetan Plateau (Fig. 1). The mean elevation of the basin is 4621 m a.s.l., ranging from 5590 m to several hundreds of meters a.s.l. The drainage area of the YZR basin is approximately 240,480 km^2, with an annual air temperature range of −0.3 to 8.8 °C for the time period 1960 to 2009 (National Meteorological Information Center, China, http://data.cma.cn/). Water discharge in the YZR basin is mainly recharged by precipitation, combined with glacier and snow melt water and ground water (Yao and Yao, 2010).

According to the topographic feature, valley shape, channel gradient, natural condition and runoff variety along the course of the YZR is divided into upstream, midstream and downstream by the Ministry of Water Resources of the People's Republic of China (MWR, PRC). Annual precipitation of the upstream, midstream and downstream of the YZR was < 300 mm, 300 to 600 mm and > 2000 mm, respectively. Detailed geographic features of each reach were listed in Fig. 1. The upper and lower reaches of the YZR basin exhibit hydrological differences due to the differences in climate, topography and land surface conditions (Liu et al., 2007; Wang et al., 2008).

According to the Genetic Soil Classification of China (GSCC), the soil order in the basin is mainly Alpine soil, which covers approximately 70% of the basin area (Zhang, 2011). The main soil types in the upper reach of the YZR basin are cold calcic soil and felty soil. The middle reach is dominated by felty soil, frigid soil and cold calcic soil, while felty soil, dark felty soil and dark brown soil persist in the lower reach. Soil texture in the basin is generally sandy loam (Zhang, 2011). Dominant vegetation of the three reaches is alpine meadow, alpine grass and alpine forest, respectively (Liu et al., 2012).

2.2. Data

There are three gauging stations located along the middle reach of the YZR, including the Lhaze, the Nugesha, and the Yangcun stations (Fig. 1). Basic information of the three gauging stations and the corresponding data are listed in Table 1. Daily discharge and SSC during 2007 to 2009 were recorded by the Lhaze, the Nugesha and the Yangcun gauging stations at three specific river cross sections along the YZR. According to the national standard “Code for liquid flow measurement in open channels” (GB 50179-93, 1993) issued by the MWR, PRC, daily discharge of a cross section was calculated by the weighted average of intraday instantaneous discharge obtained by water levels combining with specific stage-discharge relation curve. Water levels were measured every two hours during high flow period, every four hours during normal flow period and every twelve hours during low flow period by a self-recording water level gauge. The stage-discharge relation curve of a specific cross section was surveyed annually through cross section geometry, water level and flow velocity investigations during high, normal and low water flow periods. According to the national standard “Code for measurements of suspended sediment in open channels” (GB 50159-92, 1992) issued by the MWR, PRC, the instantaneous *SSC* sample was collected by a strip sampler at 60% of water depth and thereafter measured by oven drying method. Daily sediment load of the cross section was calculated by weighted average of instantaneous *SSC* and *Q*. The investigations of *SSC* were carried out while the variation of water level reaches 3% during high and normal water flow periods, and every 3–5 days during low flow period. Subsequently, *SSLs* were calculated by adding up products of paired daily discharge and *SSC* during specified time periods.

Since continuously or near-continuously discharge measurements in a river are much easier than high-frequency *SSC* measurements, accurate SRCs obtained under different flow regimes can be used to estimate *SSC* and *SSL* more frequently with discharge measurement data. It is important to ascertain whether or not the hydrological regime during the investigation period is representative, by comparing annual precipitation with the long term mean. Daily precipitation data were recorded at eleven meteorological stations within the study area (National Meteorological Information Center, China, http://data.cma.cn/). Station names and locations are depicted in Fig. 1. Precipitation data in the upstream of the three gauging stations were estimated by

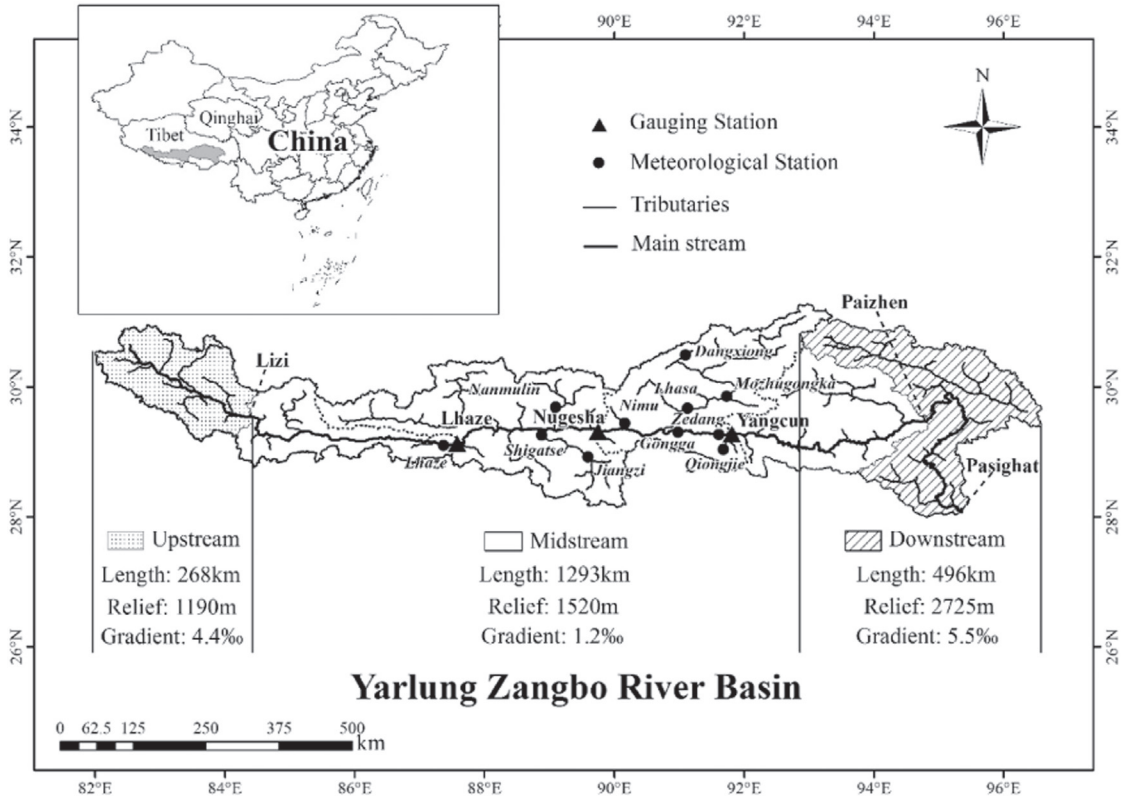

Fig. 1. The Yarlung Zangbo River basin.

the average value of meteorological stations within the catchment area, showing that precipitation in the upstream of the Lhaze, the Nugesha and the Yangcun stations were 375.3 mm, 426.5 mm and 475.3 mm in 2007, 449.9 mm, 516.9 mm and 542.3 mm in 2008, and 168.0 mm, 275.2 mm, and 304.7 mm in 2009, respectively. Comparing with the historical mean (330.1 ± 95.6 mm, 386.0 ± 91.2 mm and 408.4 ± 85.9 mm for the Lhaze, the Nugesha and the Yangcun stations, respectively). The precipitations of the three stations in 2007 were within the historical mean ± SD, but higher than the historical mean plus SD in 2008 and lower than the historical mean minus SD in 2009. Therefore, the study period of the three years is considered to cover a normal year (2007), a relative wet year (2008) and a relative dry year (2009).

3. Methods

In the present study, the traditional SRC method $SSC = aQ^b$ was chosen with regression coefficients a and b estimated by nonlinear least squares regression. Coefficient a generally represents soil erodibility and sediment source availability, and high a values indicate intensively weathered materials that can be easily eroded. Coefficient b has been generally assumed to represent erosive power, and large b values indicate a slight increase in discharge that can result in a strong increase in sediment transport. The SRCs were estimated based on all the available *Q-SSC* data from 2007 to 2009, allowing a more representative range of paired *Q-SSC* values to be analyzed and providing a greater benefit than the potential loss of accuracy associated with introducing rating curve representative (Harrington and Harrington, 2013).

Table 1
Discharge and suspended sediment concentration measurement periods, catchment areas, and average discharges, suspended sediment loads and precipitations for the three gauging stations.

Station	Measurement period		Catchmentarea (10 km^2)[d]	Discharge (10^8m/yr)[c]		*SSL*[a] (10 t/yr)[f]		Precipitation[b] (mm/yr)	
	Year	Month		All[c]	RP[d]	All[c]	RP[d]	All[c]	RP[d]
Lhaze	2007–2009	Jan.–Dec.	4.8	51.7	34.3	1.9	1.7	330.1	318.5
Nugesha	2007–2009	Jan.–Dec.[e] May–Oct.[f]	10.6	158.1	112.4	12.2	10.9	386.0	362.1
Yangcun	2007–2009	Jan.–Dec.	15.2	305.8	219.9	17.2	15.2	408.4	363.1

[a] *SSL* means suspended sediment load was calculated by the sum of the products of paired daily discharge and suspended sediment concentration during specified time periods. Relative errors of estimated *SSL* were within 10–13%;
[b] Precipitation data were obtained by the average value of meteorological stations within each catchment section;
[c] All refers to the entire observation periods in a year;
[d] RP refers to rainy periods of June to September;
[e] For discharge data;
[f] For suspended sediment concentration data.

For seasonal classes, four separate rating curves were developed including the spring (March, April and May), the summer (June, July and August), the autumn (September, October and November) and the winter (December, January, February). For discharge classes, four separate rating curves were developed for each quarter of the peak flow, i.e. 0–25%, 25–50%, 50–75%, and 75–100%. For discharge stages, two rating curves separated by discharge peaks, as described by Delmas et al. (2011) were obtained for the rising and falling limbs. Besides, *Q-SSC* datasets subdivision methods based on flood ranks and *SSC* stages were proposed and compared with the traditional SRC methods.

3.1. Subdivision based on flood ranks

For flood ranking, the exact beginning and ending dates of an annual flooding period is determined according to a critical discharge value (CDV), i.e. the lowest discharge at each gauging station during rainy periods, corresponding to 269, 844, and 1800 m^3/s for the Lhaze, the Nugesha, and the Yangcun stations, respectively. The time periods before and after the flooding period with discharge lower than the CDV, i.e. the non-flooding periods, were both assigned as flood rank0. Each year, flood rank1 began when discharge exceeded the CDV, and continued as discharge reached a peak value, then decreased and varied before increasing and reaching the peak value again. Accordingly, the following flood ranks began when the discharge exceeded the peak flow of the preceding flood rank, and ended when discharge exceeded their own peak flow, or a value lower than the CDV. For example, flood rank2 began when discharge exceeded the peak flow of flood rank1 and ended when discharge reached its own peak flow (Fig. 2). Dates of flood ranks at each station during 2007 to 2009 are listed in Table S1.

3.2. Subdivision based on SSC stages

The dates of *SSC* peaks for separating *SSC* rising and falling limbs were based on the accumulated precipitation averaged within the catchment area of each station. The *SSC* peak dates were compared with the dates of 1-day and multi-day accumulated precipitation peaks within the catchment area of each gauging station to estimate lag times (Table S2). First, the numbers of days, i.e. the length of accumulated precipitation, were selected according to the least Average Absolute Difference (AAD) values between the dates of accumulated precipitation peaks and *SSC* peaks. Second, the dates of the selected accumulated precipitation peaks were corrected by the corresponding Average Lag Times (ALT) with the dates of *SSC* peaks to obtain the estimation of *SSC* peak dates.

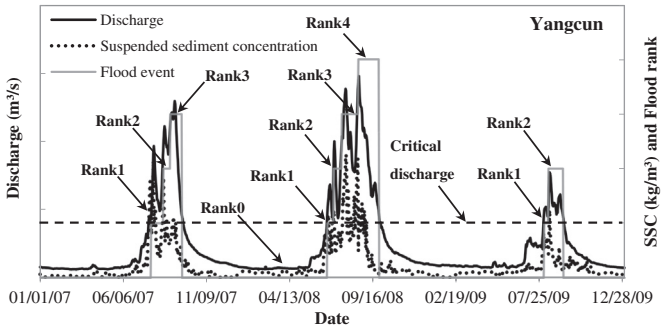

Fig. 2. Schematic diagram of the subdivision by flood ranks. First, the annual flooding period is determined according to a critical discharge value (dashed line) for each gauging station. Flood rank1 began when discharge exceeded the critical discharge value, and continued as discharge reached a peak value, then decreased and varied before increasing and reaching the peak value again. Accordingly, the following flood ranks began when the discharge exceeded the peak flow of the preceding flood rank and end when discharge exceeded their own peak flow, or a value lower than the critical discharge value. The time periods before and after the flooding period were both referred as flood rank0.

The *SSC* peak dates during different flood ranks were first compared to the dates of 1-day, 2-day, 3-day, 4-day and 5-day accumulated precipitation peaks and evaluated according to the absolute difference values with the *SSC* peak dates. The length of accumulated precipitation that had the least AAD values with corresponding *SSC* peak dates (i.e., 2.3, 8.1 and 6.4 days for the Lhaze, the Nugesha and the Yangcun stations, respectively) was identified as 2-day, 3-day and 4-day at the Lhaze, the Nugesha and the Yangcun stations, respectively (Table S2). Subsequently, the *SSC* peaks dates were estimated as the peak dates of 2-day, 3-day and 4-day accumulated precipitation during different flood ranks and corrected by the corresponding ALT of − 2 days, 1 day and 2 days for the Lhaze, the Nugesha and the Yangcun stations, respectively. The regression coefficients *a* and *b* were then estimated for both the rising and falling limbs, separated by the *SSC* peak dates estimated using accumulated precipitation.

3.3. Subdivision based on the combination of flood ranks and SSC stages (FR & SSCS)

In addition to the discharge, availability of sediment sources, erosion type such as sheet wash, gully and rill erosion and channel bank erosion could be other impact factor of *SSL* under different conditions (De Girolamo et al., 2015). As a result, in addition to subdivision separately by flood ranks (FR) and *SSC* stages (SSCS), we also combined these two methods by further dividing each flood rank dataset into *SSC* rising and falling limbs, and then developed separate SRCs for each subgroup of data.

3.4. Evaluation criteria

As suggested by Harrington and Harrington (2013), evaluation of a rating curve should not only be based on a goodness-of-fit indicator of *SSC*, but also be compared to the true load calculated by the observed *Q-SSC* dataset to identify a good predictor. In this study, the coefficient of determination (R^2), Nash-Sutcliffe efficiency coefficient (NSE), bias (BIAS) and root-mean-square error (RMSE) were utilized as evaluation criteria to compare the suitability of the proposed methods for both *SSC* and *SSL* estimation in the middle reach of the YZR with existing methods. These are defined as:

$$R^2 = \left(\frac{\sum_{i=1}^{N} (X_i - \overline{X_i})(X_{oi} - \overline{X_{oi}})}{\sqrt{\sum_{i=1}^{N} (X_i - \overline{X_i})^2 \cdot \sum_{i=1}^{N} (X_{oi} - \overline{X_{oi}})^2}} \right)^2 \quad (2)$$

$$NSE = 1 - \frac{\sum_{i=1}^{N} (X_{oi} - X_i)^2}{\sum_{i=1}^{N} (X_{oi} - \overline{X_{oi}})^2} \quad (3)$$

$$BIAS = \frac{\sum_{i=1}^{N} (X_i - X_{oi})}{N} \quad (4)$$

$$RMSE = \sqrt{\frac{1}{N} \sum_{i=1}^{N} (X_i - X_{oi})^2} \quad (5)$$

where X_i and X_{oi} are estimation and observation values, respectively. The daily *SSL*, were calculated by multiplying the observed *SSC* by the observed discharge. $\overline{X_i}$ and $\overline{X_{oi}}$ are the average estimation and observation values, respectively.

4. Results

4.1. Hydrological characteristics of the study basin

Table 1 showed that the precipitation during the rainy periods in 2007 to 2009 accounted for 96.5%, 93.8%, and 88.9% of the annual precipitation, rainy period discharge accounted for 66.3%, 71.1%, and 71.9% of the annual discharge, and rainy period *SSL* accounted for

Table 2
Statistical analyses results of the original sediment rating curve (SRC), traditional subdivision methods and the proposed subdivision methods for suspended sediment load for the entire observation periods at the three gauging stations during 2007 to 2009.

Station	Method	R^2	NSE	BIAS	RMSE
				(10^3t/d)	(10^3t/d)
Lhaze	Traditional SRC	0.74	0.10	− 1.8	8.4
	Seasonal classes	0.71	0.63	− 0.9	8.2
	Discharge classes	0.70	0.67	− 0.9	8.1
	Discharge stages	0.64	0.48	− 1.4	8.8
	Flood ranks	0.78	0.68	− 0.8	6.8
	SSC stages	0.79	0.71	− 0.6	6.6
	FR & SSCS	0.81	0.73	− 0.6	6.4
Nugesha	Traditional SRC	0.72	0.06	− 19.9	73.9
	Seasonal classes	0.74	0.62	− 4.6	63.0
	Discharge classes	0.68	0.48	− 13.0	70.7
	Discharge stages	0.59	0.51	− 11.7	81.7
	Flood ranks	0.75	0.67	− 7.3	61.6
	SSC stages	0.79	0.73	− 5.5	55.9
	FR & SSCS	0.85	0.79	− 4.0	47.6
Yangcun	Traditional SRC	0.82	0.60	− 8.4	57.6
	Seasonal classes	0.79	0.60	− 11.1	50.4
	Discharge classes	0.81	0.67	− 7.3	56.3
	Discharge stages	0.82	0.39	− 12.7	63.2
	Flood ranks	0.85	0.80	− 4.0	49.1
	SSC stages	0.88	0.83	− 3.6	44.4
	FR & SSCS	0.89	0.83	− 3.4	43.9

Table 3
Statistical analyses results of the original sediment rating curve (SRC), traditional subdivision methods and the proposed subdivision methods for suspended sediment load for the flooding periods at the three gauging stations during 2007 to 2009.

Station	Method	R^2	NSE	BIAS	RMSE
				(10^3t/d)	(10^3t/d)
Lhaze	Traditional SRC	0.52	0.74	− 9.5	20.0
	Seasonal classes	0.52	0.71	− 4.7	17.8
	Discharge classes	0.56	0.80	− 3.2	17.2
	Discharge stages	0.58	0.79	− 3.5	16.5
	Flood ranks	0.60	0.80	− 3.1	16.0
	SSC stages	0.61	0.81	− 2.8	15.6
	FR & SSCS	0.64	0.82	− 2.8	15.1
Nugesha	Traditional SRC	0.56	0.73	− 51.8	121.5
	Seasonal classes	0.56	0.78	− 19.2	106.6
	Discharge classes	0.55	0.77	− 37.7	112.4
	Discharge stages	0.55	0.77	− 32.8	110.6
	Flood ranks	0.61	0.80	− 13.8	100.2
	SSC stages	0.68	0.83	− 11.4	90.7
	FR & SSCS	0.76	0.86	− 9.7	79.8
Yangcun	Traditional SRC	0.65	0.80	− 42.0	134.8
	Seasonal classes	0.65	0.81	− 27.4	126.5
	Discharge classes	0.66	0.81	− 27.0	125.0
	Discharge stages	0.67	0.82	− 25.6	123.0
	Flood ranks	0.70	0.86	− 15.3	113.7
	SSC stages	0.77	0.88	− 15.5	102.3
	FR & SSCS	0.80	0.91	− 8.9	85.6

89.5%, 89.3%, and 88.4% of the annual *SSL* for the Lhaze, the Nugesha, and the Yangcun gauging stations, respectively. These mainly caused by the impact of the summer southwest monsoon in the middle reach of the YZR that most of the annual precipitation occurred during the rainy period from June to September (Liu et al., 2007; Jia et al., 2008). Therefore, the rainy period is a key for a more precise estimation of *SSL* in the study basin.

4.2. SSC and SSL estimation of the proposed methods for the whole period

The traditional SRC method without subdivision (Walling, 1974), and the subdivision methods based on seasonal classes (Walling, 1977), discharge stages (Preston et al., 1989; De Girolamo et al., 2015) and discharge classes (Delmas et al., 2011), and the proposed subdivision methods based on flood ranks and *SSC* stages, and the combination of FR & SSCS were compared for *SSC* (Fig. S1) and *SSL* estimation (Table 2) for the entire observation period at each station.

Compared to the original SRC and traditional subdivision methods, the newly proposed subdivision methods showed better performance in estimating both *SSC* and *SSL*, with higher R^2 and NSEs, and lower BIASs and RMSEs (Fig. S1 and Table 2). As shown in Table 2, the proposed subdivision methods improved R^2 of *SSL* estimation by 0.07–0.17, 0.01–0.26 and 0.03–0.10, increased NSEs of *SSL* estimation by 0.01–0.25, 0.05–0.31 and 0.13–0.44, lowered BIASs of *SSL* estimation by 1.9–15.5%, 0.0–14.0% and 5.9–17.6%, and reduced RMSEs of *SSL* estimation by 25.1–46.4%, 2.2–53.2% and 2.8–41.0% for the Lhaze station, the Nugesha station and the Yangcun station, respectively. The most accurate sediment concentration and load estimation for the entire observation period was obtained using the combination of FR & SSCS method.

4.3. SSC and SSL estimation of the proposed methods for the flooding periods

The flooding periods, accounting for a majority of the annual *SSL* at the three stations in the middle reach of the YZR, were selected to evaluate flood ranks, *SSC* stages and FR & SSCS methods against the traditional SRC and traditional subdivision methods for *SSC* (Fig. S2) and *SSL* estimation (Table 3).

Overall, the newly proposed subdivision methods showed better performance in estimation results of both *SSC* and *SSL* than the original SRC and traditional subdivision methods for the flooding period (Fig. S2 and Table 3). As shown in Table 3, the proposed subdivision methods improved R^2 of *SSL* estimation by 0.02–0.12 0.05–0.21 and 0.03–0.15, increased NSEs of *SSL* estimation by 0.00–0.11, 0.02–0.09 and 0.04–0.10, lowered BIASs of *SSL* estimation by 0.4–7.0%, 3.1–16.3% and 4.0–7.4%, and reduced RMSEs of *SSL* estimation by 1.8–9.9%, 3.7–19.0% and 4.0–17.5% for the three stations, respectively. Same as that observed for the entire time period, the most accurate *SSC* and *SSL* estimator was FR & SSCS for the flooding period.

5. Discussion

5.1. Hypotheses of the proposed subdivision methods

The YZR located on the northern slope of the Himalayan Mountains, i.e. part of the Brahmaputra River in China, is the longest and most important river in Tibet. The YZR basin experiences some of the most serious soil erosion problems on the Tibetan Plateau (Wen et al., 2000). Meanwhile, the middle reach of the basin includes one of the most fertile and populous agriculture regions in Tibet (Li et al., 2008). However, due to the unique climate, topography and landform features, the traditional SRC subdivision methods, e.g. seasonal and hydrological groupings, were not adequate and need to be improved while applied in the YZR basin.

The traditional SRC subdivision methods grouping *Q-SSC* datasets by discharge classes employed flow magnitude, duration, frequency, timing and rate of change as the thresholds (Stromberg et al., 2007). Among these practices, subdivision of low and high flow were widely reported in literature (Preston et al., 1989; De Girolamo et al., 2015), inferring that higher water flow with larger erosive power can mobilize sediment sources with less erodibility or not available during lower flows. In the middle reach of the YZR basin, the hydrological regime also plays an important role in the suspended sediment transport. As mentioned previously, *SSLs* during rainy periods at the study stations accounted for nearly 90% of the annual loads. Meanwhile, the variations of discharge and *SSC* from 2007 to 2009 showed that even equivalent discharge may have different magnitudes of *SSC* (Fig. 3), for

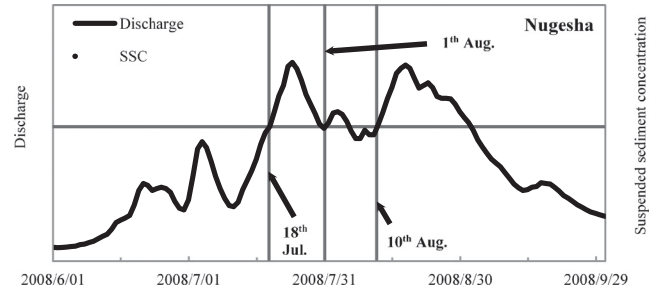

Fig. 3. Schematic diagram of suspended sediment concentrations (*SSCs*) under equivalent discharge.

example the discharge and corresponding *SSCs* in the falling limb on 6 July 2008 (3730 $m^3 \cdot s^{-1}$; 0.544 $kg \cdot m^{-3}$), 6 August 2008 (3810 $m^3 \cdot s^{-1}$; 1.08 $kg \cdot m^{-3}$) and 5 September 2008 (3850 $m^3 \cdot s^{-1}$; 0.382 $kg \cdot m^{-3}$) at the Yangcun station, and in the rising limb on 18 July 2008 (2000 $m^3 \cdot s^{-1}$; 1.64 $kg \cdot m^{-3}$), 1 August 2008 (2070 $m^3 \cdot s^{-1}$; 4.11 $kg \cdot m^{-3}$) and 10 August 2008 (1970 $m^3 \cdot s^{-1}$; 0.995 $kg \cdot m^{-3}$) at the Nugesha station. The differing magnitudes of *SSC* in period of equivalent discharge may be due to additional controlling factors such as the difference in precipitation pattern, antecedent soil moisture contents, or water from different sediment source areas (Zeng et al., 2011; De Girolamo et al., 2015). Availability of sediment sources depends not only on erosive flow but also on the pre-conditions. Therefore, we subdivided SRCs by flood ranks.

The traditional SRC subdivision methods of grouping *Q-SSC* datasets by discharge stages (rising and falling limbs) have been previously reported in literatures (Walling, 1977; Delmas et al., 2011). However, a temporal disconnect was observed between the *SSC* peak and the discharge peak, referred to as clockwise or counterclockwise hysteresis, in the middle reach of the YZR (Fig. 4). For example, the dates of discharge peaks and *SSC* peaks during different flood ranks in 2008 were 21 June and 24 June (rank1), 4 July and 3 July (rank2), and 24 July and 6 August (rank3) at the Nugesha station, with a maximum difference of 12 days between the peak flow and the peak *SSC*. The large observed difference in hysteresis occurrences at the three stations implied that sediment transport started immediately when rainfall excess was generated (Sadeghi et al., 2008). This resulted in inaccurate estimation of *SSC* by traditional discharge stage subdivisions. Therefore, a new subdivision method of grouping *Q-SSC* datasets by *SSC* stages, i.e. the rising and falling limbs of *SSC*, instead of discharge, was developed for this study. Separating the *SSC* rising and falling limbs required estimation of the dates of *SSC* peaks.

According to previous studies, precipitation is the main water source in the YZR basin in summer (Yao and Yao, 2010; Yang et al., 2014). Table 1 also shows that most of the discharge and *SSL* occurred during the rainy periods (from June to September). Therefore, it can be inferred that precipitation is the dominating driving force of sediment

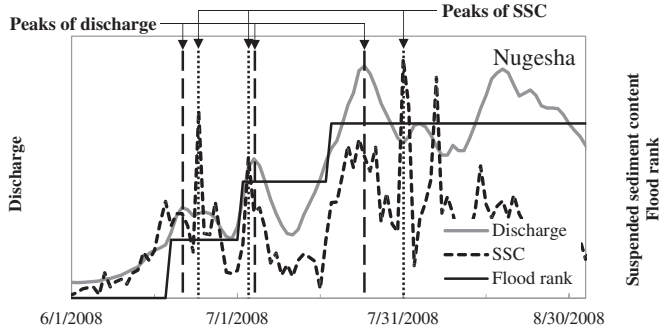

Fig. 4. Schematic diagram of different peak dates of discharge and suspended sediment concentration (*SSC*) under different flood ranks.

erosion and transport processes in the study basin especially during the flooding periods (within the rainy periods). When rainfall intensity is high, water discharge could be mainly generated by infiltration excess and cause the flushing of sediment previously accumulated on the river bed, resulting in higher *SSC* during the rising limb than equivalent discharge in the falling limb (De Girolamo et al., 2015). Based on the assumption that precipitation-driven erosion is closely related to precipitation and pre-conditions in the YZR basin, estimation of the date of *SSC* peaks was based on information of accumulated precipitation peaks for this study.

5.2. Evaluating the proposed subdivision methods

Traditional subdivision methods based on seasonal classes, discharge stages and discharge classes have limitations in use for the middle reach of the YZR basin. For example, *SSC* data is quite limited for spring, fall and winter for seasonal classification at the Nugesha station. For subdivision by changing stages, variation of *SSC* did not closely match the discharge change. For separation by discharge levels, the data showed that equivalent discharge may have different magnitudes of *SSC*, illustrating that sediment availability may depend on the pre-conditions such as soil moisture etc.

Among the traditional SRC and subdivision methods, most of the traditional subdivision methods exhibited better estimation results than the traditional SRC method. Among the traditional subdivision methods, seasonal classes and discharge stages showed better estimation of *SSC* than discharge classes. However, some traditional subdivision methods, i.e. discharge stages classes at the Yangcun station, showed poorer estimation of *SSL* compared to the traditional SRC method (Table 2). This suggests that inappropriate subdivision of datasets may not achieve better estimation.

In present study, compared to the traditional SRC and traditional subdivision methods, the proposed subdivision methods all presented better performance in estimating both *SSC* and *SSL* for both the whole observation period and the flooding period, have higher R^2 and NSE and lower BIAS and RMSE, indicating that the proposed subdivision methods are effective and rational.

As shown in Fig. 5, although the number of fitting data (N) for higher flood ranks (rank3 and rank4) was limited due to the infrequent high flow conditions, R^2 values were higher with the increasing flood ranks for the three gauging stations. The potential reason is that, most sediment source remaining from previous year and activated by soil thawing in spring was eroded and transported in early flood events, the remaining soil particles in the source area are less erodible and at the same time further stabilized by the increasing vegetation coverage. As a result, higher discharge in later flood events might transport coarse-grained bed material which could not be mobilized during early flood. Since transport of coarse-grained particles depends highly on water flow (Hudson, 2003), correlations between discharge and *SSC* became higher in later flood ranks. This result providing additional evidence for the reasonability of the proposed subdivision method by flood ranks.

5.3. Regression coefficients of the proposed subdivision methods

According to the literature (Asselman, 2000), the values of the regression coefficients (*a* and *b*) are related to the erosion severity, the sediment availability, and the power of the river flow to erode and transport the available material. In this study, with increasing flood rank, regression coefficient *a* had a decreasing trend, while coefficient *b* had an increasing trend for all the three gauging stations (Fig. 5). The *Q* and *SSC* variation with flood ranks support the variation of *a* and *b* with different hydrological conditions. Since peak flow increased with increasing flood rank, the variation trends of the regression coefficients for different flood ranks illustrated higher erosive power associated with the higher discharge and lower erodibility of remaining sediment for higher flood ranks. In addition, high *b* values may be also related to

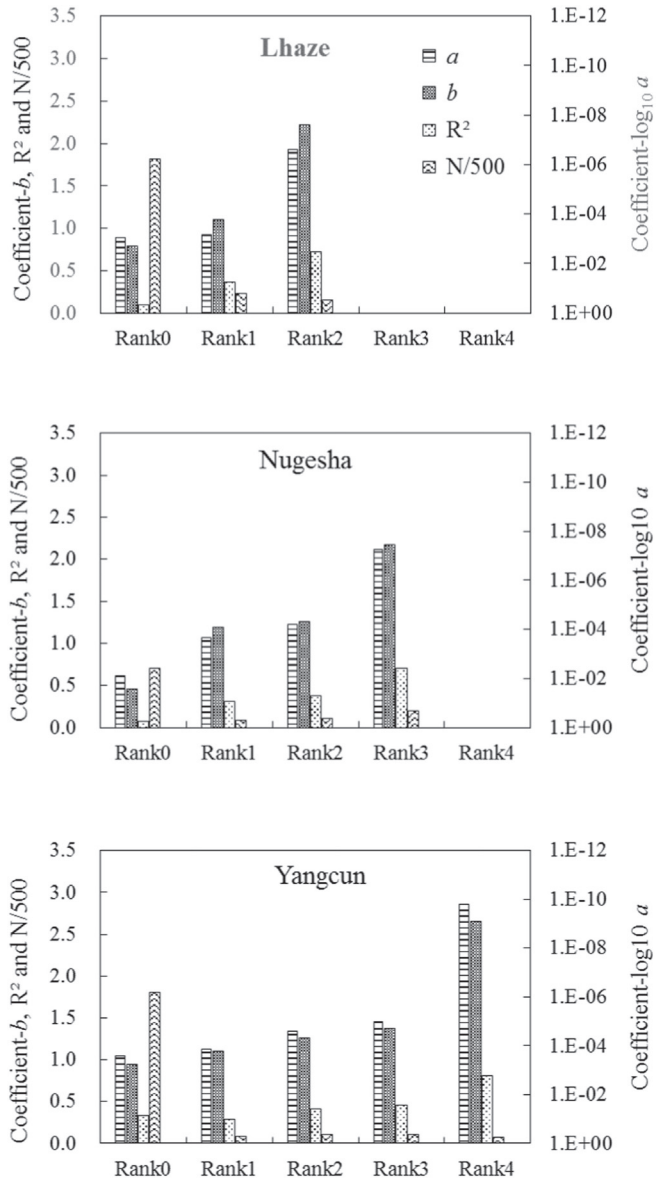

Fig. 5. Regression coefficients of suspended sediment concentration for flood rank subdivision with increasing floods (The axis of $\log_{10}a$ is reversed).

the coarse sediment during higher floods since the powerful flow is more important for the transport of sand compared to silt and clay (Walling, 1974). Investigation on sediment grain distribution is thus suggested for future research on sediment dynamics in the study area since it could be a good indicator to further explain the proposed sediment rating curves.

The average coefficient *a* for the falling limbs of *SSC* was always lower than for the rising limbs, while the average coefficient *b* for the falling limbs was higher than for the rising limbs at the three gauging stations (Table 4). These can be attributed to differing availability of sediment source, erosive power and sediment transport capacity under various *SSC* stages, which are closely related to accumulated precipitation within the catchment area. During the rising limb with increasing precipitation, overland flow carried more suspended sediment to the river channel, resulting in higher *SSC*. During the falling limb with decreasing precipitation, overland flow supplied less suspended sediment and diluted the *SSC* in the river. Consequently, discharge in the river carried more sediment for the rising limb than for the falling limb with same discharge.

Correlation between the regression coefficients *a* and *b* for flood

Table 4
Regression coefficients of sediment rating curve for suspended sediment concentration stage subdivision at the three gauging stations in the middle reach of the Yarlung Zangbo River.

Station	Stage	*a*	*b*	R^2	*N*	Sig.
Lhaze	Falling	1.40E − 07	2.33	0.69	98	1.86E − 13**
	Rising	1.72E − 04	1.34	0.38	89	4.06E − 10**
Nugesha	Falling	3.54E − 06	1.68	0.59	139	3.38E − 15**
	Rising	2.97E − 04	1.05	0.25	58	4.72E − 04**
Yangcun	Falling	1.79E − 05	1.29	0.35	159	8.50E − 15**
	Rising	6.08E − 03	0.61	0.24	32	1.36E − 03**

** Refer to the significant level of 0.01 ($p < 0.01$).

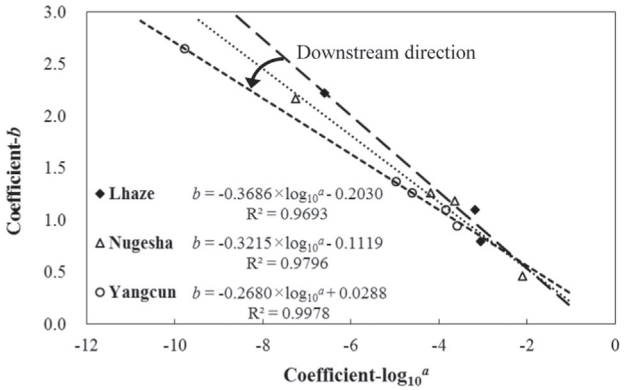

Fig. 6. Correlation between the coefficients of the sediment rating curves subdivided using flood ranks in the middle reach of the YZR River basin.

ranks were plotted in Fig. 6. The observed negative correlations between the regression coefficients in the study basin have also been reported in other regions (Syvitski et al., 2000; Ali and Boer, 2007). Since coefficients *a* and *b* were often found to be inversely correlated, Asselman (2000) proposed that it is more appropriate to use a combination of the *a* and *b* values, i.e. the steepness of the rating curve, as a comprehensive measure of soil erodibility and river flow erosivity.

The slopes of the correlations between coefficients *b* and $\log_{10}a$ become "flat" along the downstream direction (Fig. 6). Steep rating curves, i.e. low *a* and high *b* values, are often characteristic for river sections where an increase in discharge results in a large increment of *SSC*. This likely indicates that either important sediment sources such as soil on river bank etc. become available when the water level rises, or the power of the river flow to erode material during high discharge periods is high. However, differences in steepness do not necessarily indicate differences in the sediment transport regime (Asselman, 2000). Statistically, a linear regression line often best fits the average values of $\log_{10}Q$ with $\log_{10}$SSC (Thomas, 1988). In this study, the slope of the fitted *b* vs $\log_{10}a$ curve is − 0.37, − 0.32, and − 0.27 at the Lhaze, the Nugesha and the Yangcun stations, respectively. These values are close to the $-1/\log_{10}Q_{ave}$ values of − 0.37, − 0.31, and − 0.28 at the Lhaze, the Nugesha and the Yangcun stations, respectively. Therefore, the steepness of the SRCs in this study are related to the scale of the catchment area and resulting river flow as reported by Asselman (2000).

5.4. Patterns of SSL transportation in the study basin

Generally, the seasonal *Q* and *SSC* regimes of the study basin exhibited positive hysteresis pattern (Fig. 7). This is similar to most large fluvial systems of the world, such as the Rhine River (Asselman, 1999), the upper Niger River (Picouet et al., 2001), the lower Fraser River (Kostaschuk et al., 1989), the lower Mississippi River (Mossa, 1996), and other rivers such as the lower Tordera (Rovira and Batalla, 2006) and the Tahiti basin (Wotling and Bouvier, 2002). This hysteresis

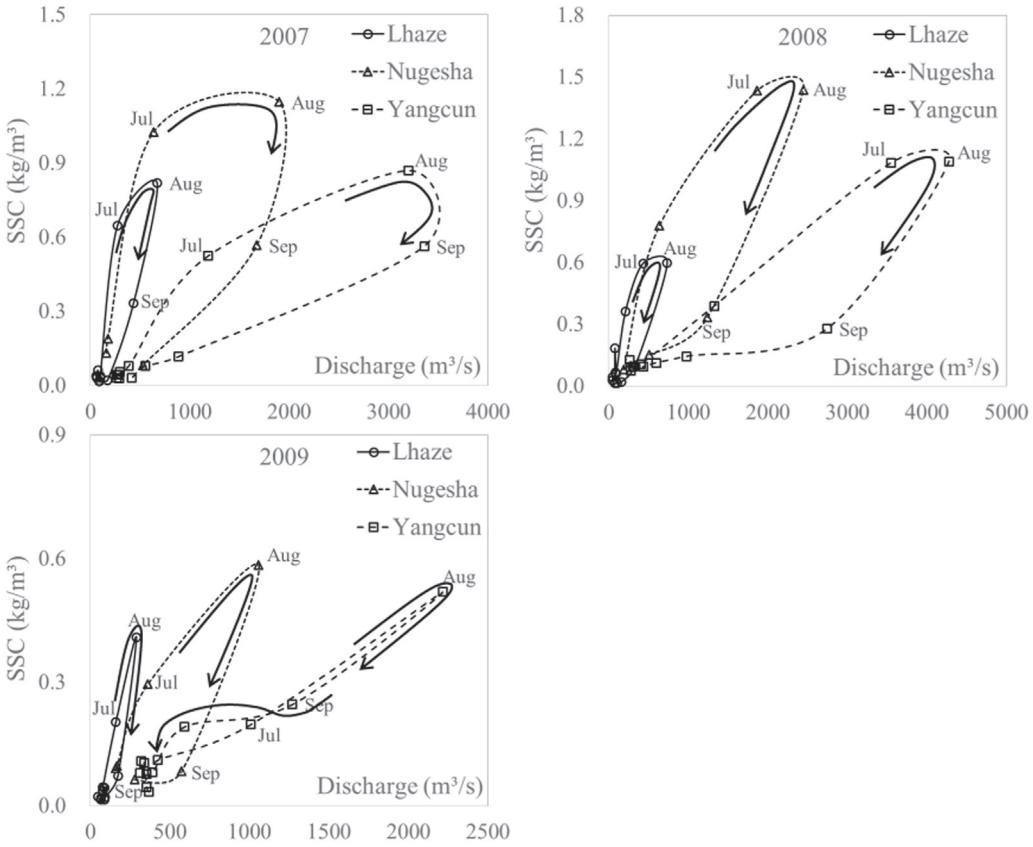

Fig. 7. Hysteresis behaviors of monthly water discharge and suspended sediment concentration (*SSC*) during 2007 to 2009 at the Lhaze, the Nugesha and the Yangcun gauging stations.

behavior suggest that *Q-SSC* relationships in the study area of the YZR basin were mainly controlled by the transport of fine-grained materials originated from distal parts of the river basin, such as glaciated areas in the upper reaches or channel scouring at gorge sections (Hudson, 2003; Gao and Josefson, 2012). Considering the sequence of flood events, most of the events exhibited positive hysteresis pattern (Fig. 8). This is likely due to the depletion effect of sediment from source areas, and the successive reduction of erosion generated by precipitation (Gao and Josefson, 2012).

For discharge stages subdivision, *SSC* for a given *Q* was higher on the rising limb than on the falling limb in most cases indicating that the river transported more sediment during early flood events due to sediment source depletion and stabilization effects. The thawing of soil in late spring activated a large amount of sediments that could be easily eroded and transported to the fluvial channel by the simultaneous increase in temperature and precipitation in early summer, while the river transported less sediments under freezing condition in the late autumn, winter, and early spring. Therefore, the higher discharge in latter flood events could only mobilize sediment source remaining from the previous flood events.

The differences of *SSC* between the rising limb and the falling limb under equivalent discharge were decreased towards downstream direction (Figs. 7 and 8). This might be due to the increasing vegetation coverage resulted from the increasing precipitation along downstream direction, and also the deposition of coarse sediment at wide valley sections along the river channel.

The sediment sources for lower mean *SSC* in later flood events at the three stations during 2007 to 2009 were mainly coarse-grained sandy bed material. This was supported by the reduction in the leading time between flood peak and *SSC* peak with sequential events (Table S2), which usually occurred due to the sand entrained from the channel bed (Hudson, 2003). These results thus infer that the flood ranks SRC subdivision method applied to the three gauging stations in present study is reasonable.

Though the discharge of the study basin was from the combination of precipitation, melt water and ground water, precipitation was still the main water source in summer. This way, seasonal *Q* and *SSC* were synchronous with the precipitation (Fig. 9). Besides, the *SSC* peak dates were highly related to the specific precipitation peak dates (Table S2), indicating that precipitation was dominate driving force of sediment production and transport processes in the study basin especially during the flooding periods. These indicate suitability of the assumption that erosion was closely related to precipitation and pre-conditions for the study basin and the *SSC* stages need to be sub-divided for a better estimate of sediment loads.

5.5. Impact of precision and resolution of datasets on the proposed subdivision methods

Daily *SSLs* from 2007 to 2009 of the three gauging stations issued by the MWR, PRC were calculated by weighted average of paired instantaneous *Q-SSC* data. As reported by the GB 50179-93, relative errors of instantaneous discharge measurement were within 5%, 6% and 9% for high, normal and low water levels, respectively, and of daily discharge estimation were within 2% for high and normal water levels and within 5% for low water level. As reported by the GB 50159–92, relative errors of instantaneous *SSC* measurement were within 8% (7% from sampling and 1% from sample treatment), and of daily *SSC* estimation were within 3%. Relative precision of *SSL* was given by the coefficient of variation (CV) as reported by Vericat and Batalla (2006) as below:

$$CV = [(\sigma C/C)^2 + (\sigma Q/Q)^2]^{1/2} \quad (6)$$

where $\sigma C/C$ and $\sigma Q/Q$ are relative error terms for the *SSC* and discharge

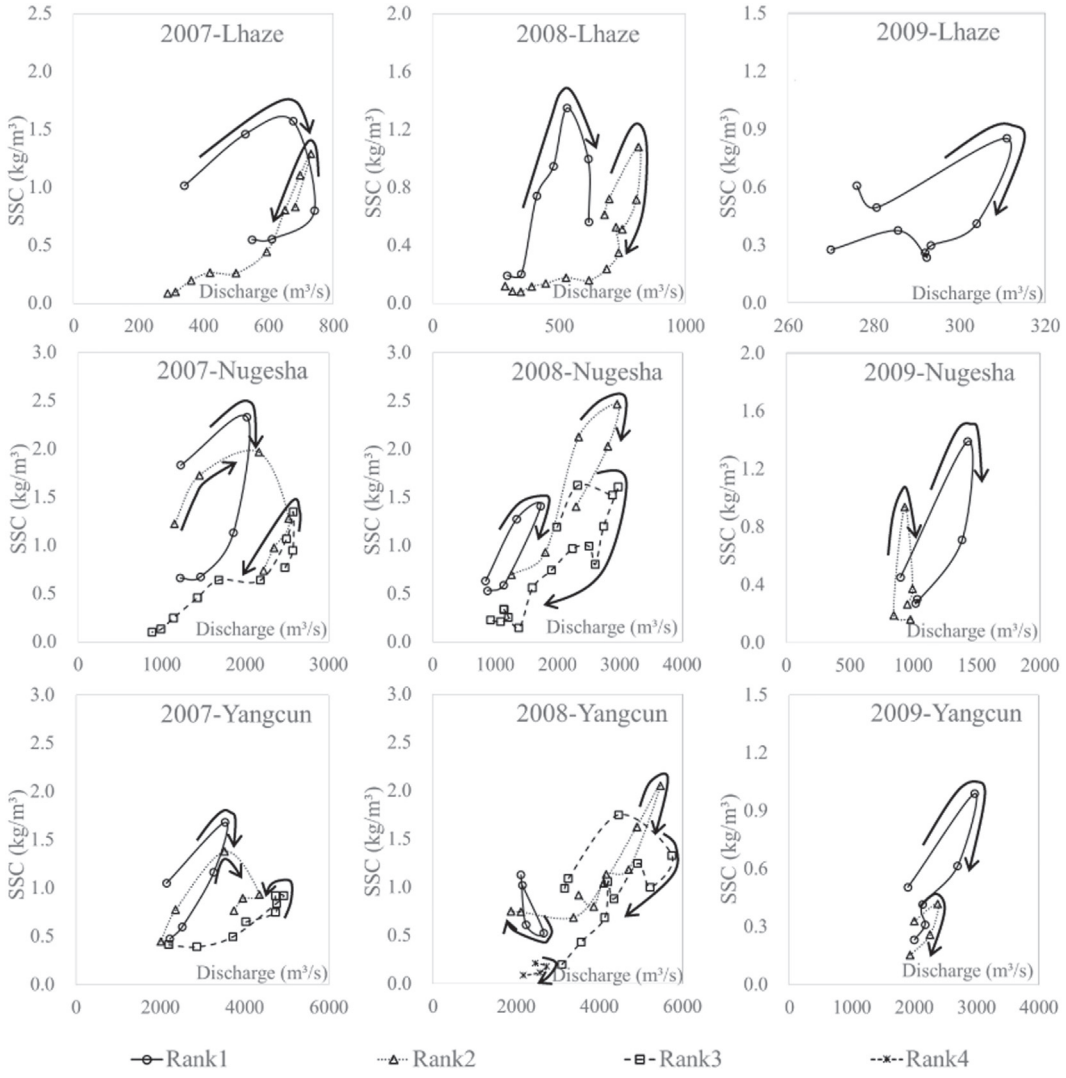

Fig. 8. Hysteresis behaviors of water discharge and suspended sediment concentration (*SSC*) with sequential events during 2007 to 2009 at the Lhaze, the Nugesha and the Yangcun gauging stations.

estimations, respectively. The CV of daily *SSL* was calculated to be 0.10 for high and normal and 0.13 for low water levels, which were closed to the values reported in previous studies. For example, Mclean et al. (1999) reported that CVs of single daily *SSL* investigated in 1968 and 1972 at three gauging stations in the lower Fraser River were 0.15. Vericat and Batalla (2006) reported that CVs of single instantaneous *SSL* investigation during 2002 to 2004 at two sections in the lower Ebro River were 0.11 and 0.21, respectively. It should be noted that, the relative precision values calculated following the criteria were the maximum limit for hydrologic data compilation required by the MWR, PRC. In fact, the actual relative precision of discharge and *SSC* determined following the criteria were much lower as reported by hydrology bureaus and gauging stations. For example, Chen et al. (2005) found that relative errors of discharge measurement at the Huanglingmiao gauging station (catchment area is about 1.0×10^6 km^2) were 2.0%, 3.6% and 3.9% for high, normal and low water levels, respectively. Wang et al. (2006) found that relative errors of daily sediment load at the Zhengyixia gauging station (catchment area is about 3.6×10^4 km^2) was 2.1% in average and 4.1% in maximum. Therefore, the precision of *SSL* derived from *Q-SSC* datasets would be < 10–13%.

Daily discharge and *SSC* datasets issued by the MWR, PRC were used to improve SRC subdivision method in this study. Previously, hourly *Q-SSC* data were also used to study the SRC (Fenn et al., 1985). Compared to daily data, hourly data have large variation ranges in *Q* and *SSC*, and can reflect more exact information of paired *Q-SSC* such as the impact of precipitation-driven runoff on sediment generation and transport, and would have higher precision due to the direct (instantaneous) measurements of *Q* and *SSC* than those flow-weighting daily average values (Holtschlag, 2001). Since hourly data can divide discharge and *SSC* peaks and calculate lag time more accurately, hourly data may have more advantage to the subdivision methods based on discharge and *SSC* stages, i.e. the traditional discharge stages and proposed *SSC* stages subdivision methods. Therefore, even though the proposed subdivision methods were developed based on daily data in this study, it can be anticipated that the estimation results will be even improved on data with shorter time intervals.

6. Conclusions

New subdivision methods were proposed in this study based on 3-year daily discharge and *SSC* data at the three gauging stations in the middle reach of the YZR basin. It is concluded through the investigation that: 1) Estimation of *SSC* and *SSL* using the newly proposed methods for both the whole observation period and the flooding period have higher R^2, much improved NSEs, smaller BIASs and lower RMSEs, indicating better performance than the traditional subdivision methods; 2) Comparing the proposed methods, *SSC* stages subdivision method generally showed better estimation than flood ranks subdivision

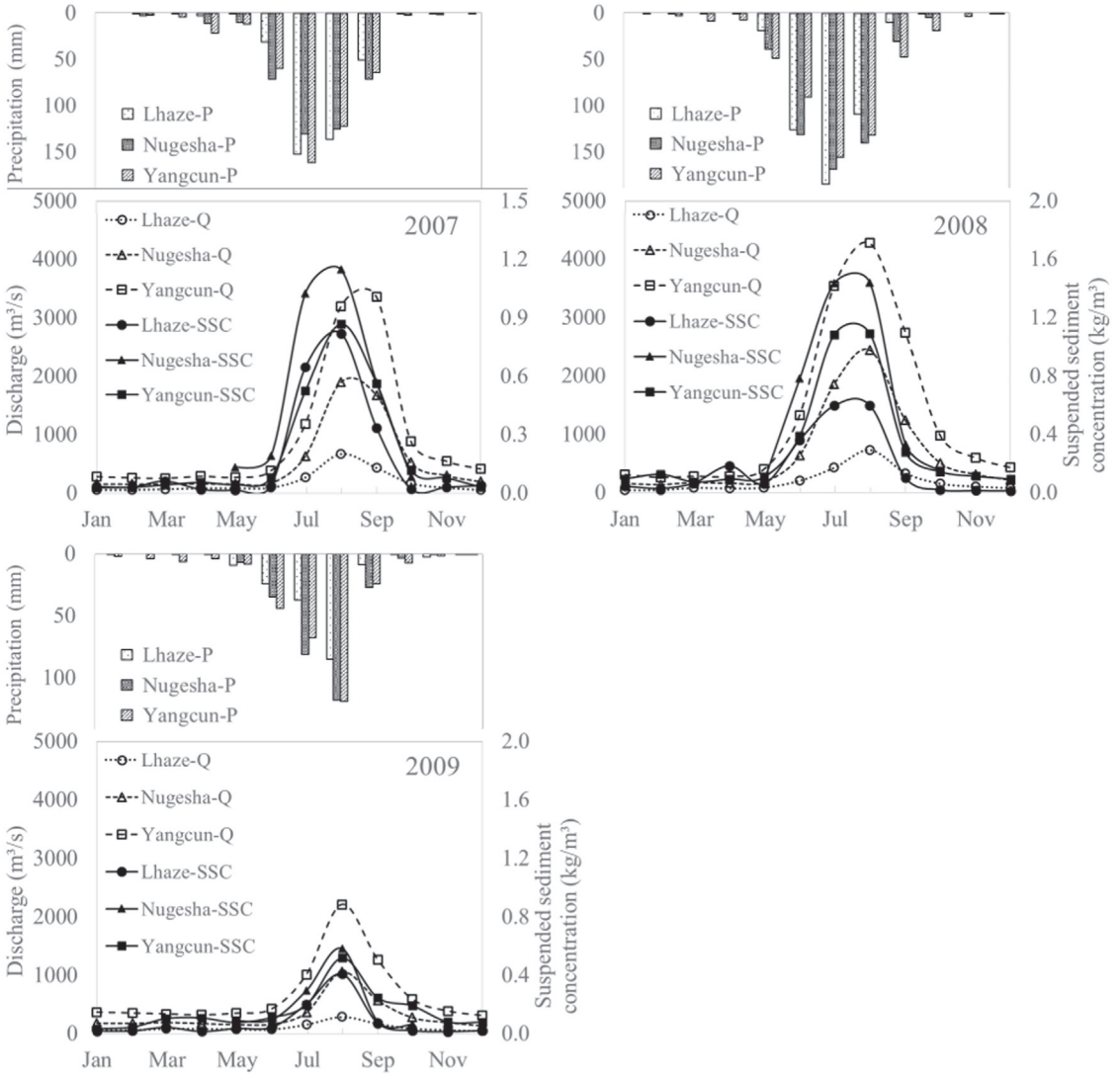

Fig. 9. Hydrograph of precipitation (*P*), seasonal water discharge (*Q*) and suspended sediment concentration (*SSC*) during 2007 to 2009 at the Lhaze, the Nugesha and the Yangcun gauging stations.

method, and the combination of the two separately proposed subdivision methods, i.e. FR & SSCS presented the best estimation for both *SSC* and *SSL*.

Acknowledgement

This work was supported by the "Strategic Priority Research Program (B)" of the Chinese Academy of Sciences (Grant No. XDB03030305), and the National Natural Science Foundation of China (Grant No. 41371087, 41401247 and 41422101).

Appendix A. Supplementary data

Supplementary data to this article can be found online at https://doi.org/10.1016/j.catena.2017.09.023.

References

Abbas, N., Subramanian, V., 1984. Erosion and sediment transport in the Ganges River basin (India). J. Hydrol. 69, 173–182.
Abdelazim, M.N., Elfiky, M.M., Owais, T.M., Nassar, M.H., 2007. Modelling of suspended sediment - in Nile River using ANN. In: International Conference on Software and Data Technologies, pp. 209–214.
Ali, K.F., Boer, D.H.D., 2007. Spatial patterns and variation of suspended sediment yield in the upper Indus River basin, northern Pakistan. J. Hydrol. 334, 368–387.
Asselman, N.E.M., 1999. Suspended sediment dynamics in a large drainage basin: the River Rhine. Hydrol. Process. 13, 1437–1450.
Asselman, N.E.M., 2000. Fitting and interpretation of sediment rating curves. J. Hydrol. 234, 228–248.
Audry, S., Schäfer, J., Blanc, G., Jouanneau, J.M., 2004. Fifty-year sedimentary record of heavy metal pollution (Cd, Zn, Cu, Pb) in the Lot River reservoirs (France). Environ. Pollut. 132, 413–426.
Beale, E.M.L., 1962. Some uses of computers in operational research. Industrielle Organ. 31, 51–52.
Chen, X.L., Wang, G.F., Niu, Z.R., 2005. Discussion on the method of calculating mean sediment concentration with partial flow weighted. Hydrology (Chinese). 25, 46–49.
Dai, Z.J., Liu, J.T., 2013. Impacts of large dams on downstream fluvial sedimentation: an example of the Three Gorges Dam (TGD) on the Changjiang (Yangtze River). J. Hydrol. 480, 10–18.
De Girolamo, A.M., Pappagallo, G., Porto, A.L., 2015. Temporal variability of suspended sediment transport and rating curves in a Mediterranean river basin: the Celone (SE Italy). Catena 128, 135–143.
Delmas, M., Cerdan, O., Cheviron, B., Mouchel, J.M., 2011. River basin sediment flux assessments. Hydrol. Process. 25, 1587–1596.
Devol, A.H., et al., 1986. Water discharge and suspended sediment concentrations in the Amazon River: 1982–1984. Water Resour. Res. 22, 756–764.
Fenn, C.R., Gurnell, A.M., Beecroft, I.R., 1985. An evaluation of the use of suspended sediment rating curves for the prediction of suspended sediment concentration in a proglacial stream. Geogr. Ann. 67, 71–82.
Gao, P., Josefson, M., 2012. Event-based suspended sediment dynamics in a central New York watershed. Geomorphology 425–437.
Harrington, S.T., Harrington, J.R., 2013. An assessment of the suspended sediment rating curve approach for load estimation on the Rivers Bandon and Owenabue, Ireland. Geomorphology 185, 27–38.

Holtschlag, D.J., 2001. Optimal estimation of suspended-sediment concentrations in streams. Hydrol. Process. 15, 1133–1155.
Horowitz, A.J., 2003. An evaluation of sediment rating curves for estimating suspended sediment concentrations for subsequent flux calculations. Hydrol. Process. 17, 3387–3409.
Hudson, P.F., 2003. Event sequence and sediment exhaustion in the lower Panuco Basin, Mexico. Catena 52, 57–76.
Jia, J.W., Lv, S.Y., Wang, Z.X., 2008. Analysis of water resources quantity characteristics of the Yaluzangbu River Basin. Yangtze River (Chinese). 17, 71–72.
Kesel, R.H., 1989. The role of the Mississippi River in wetland loss in southeastern Louisiana, U.S.A. Environ. Geol. Water Sci. 13, 183–193.
Kostaschuk, R.A., Luternauer, J.L., Church, M.A., 1989. Suspended sediment hysteresis in a salt-wedge estuary: Fraser River, Canada. Mar. Geol. 87, 273–285.
Lal, R., 2003. Soil erosion and the global carbon budget. Environ. Int. 29, 437–450.
Li, Z.L., Xu, Z.X., Gong, T.L., 2008. Characteristics of runoff variation in the Yarlung Zangbo River basin. Geogr. Res. (Chinese) 27, 353–361.
Liu, Z.F., Tian, L.D., Yao, T.D., Gong, T.L., Yin, C.L., Yu, W.S., 2007. Variations of δ18O in precipitation of the Yarlung Zangbo River Basin. Acta Geographica Sinica (Chinese) 17, 317–326.
Liu, Z., Yao, Z., Huang, H., Wu, S., Liu, G., 2012. Land use and climate changes and their impacts on runoff in the Yarlung zangbo river basin, China. Land Degrad. Dev. 25, 203–215.
Lu, X.X., Siew, R.Y., 2006. Water discharge and sediment flux changes over the past decades in the Lower Mekong River: possible impacts of the Chinese dams. Hydrol. Earth Syst. Sci. 10, 181–195.
Mclean, D.G., Church, M., Tassone, B., 1999. Sediment transport along lower Fraser River: 1. Measurements and hydraulic computations. Water Resour. Res. 35, 2533–2548.
Mei, X., Dai, Z., Gelder, P.H.A.J.M., Gao, J., 2015. Linking Three Gorges Dam and downstream hydrological regimes along the Yangtze River, China. Earth Space Sci. 2, 94–106.
Milliman, J.D., Farnsworth, K.L., 2011. River Discharge to the Coastal Ocean-A Global Synthesis. Cambridge University Press, Cambridge, UK.
Mladenovic, M.B., Kolarov, V., Damjanovic, V., 2013. Sediment regime of the Danube River in Serbia. Int. J. Sediment Res. 28, 470–485.
Morgan, R.P.C., 1995. Soil Erosion and Conservation, 2nd ed. Longman Scientific & Technical London.
Mossa, J., 1996. Sediment dynamics in the lowermost Mississippi River. Eng. Geol. 45, 457–479.
Peters-Kümmerly, B.E., 1973. Untersuchungen über zusammensetzung und transport von Schwebstoffen in einigen Schweizer Flüssen. Eclogae Geol. Helv. 28, 137–151.
Picouet, C., Hingray, B., Olivry, J.C., 2001. Empirical and conceptual modelling of the suspended sediment dynamics in a large tropical African river: the Upper Niger river basin. J. Hydrol. 250, 19–39.
Preston, S.D., Bierman, V.J., Silliman, S.E., 1989. An evaluation of methods for the estimation of tributary mass loads. Water Resour. Res. 25, 1379–1389.
Quilbé, R., et al., 2006. Selecting a calculation method to estimate sediment and nutrient loads in streams: application to the Beaurivage River (Québec, Canada). J. Hydrol. 326, 295–310.
Rovira, A., Batalla, R.J., 2006. Temporal distribution of suspended sediment transport in a Mediterranean basin: the Lower Tordera (NE SPAIN). Geomorphology 79, 58–71.
Sadeghi, S.H.R., et al., 2008. Development, evaluation and interpretation of sediment rating curves for a Japanese small mountainous reforested watershed. Geoderma 144, 198–211.
Schäfer, J., et al., 2002. Ten-year observation of the gironde tributary fluvial system: fluxes of suspended matter, particulate organic carbon and cadmium. Mar. Chem. 79, 229–242.
Shi, C.X., 2015. Decadal trends and causes of sedimentation in the Inner Mongolia reach of the upper Yellow River, China. Hydrol. Process. 84, 2461–2468.
Sivakumar, B., Chen, J., 2006. Suspended sediment load transport in the Mississippi River basin at St. Louis: temporal scaling and nonlinear determinism. Earth Surf. Process. Landf. 32, 269–280.
Stromberg, J.C., Champ, V.B., Dixon, M.D., Lite, S.J., Paradzick, C., 2007. Importance of low-flow and high-flow characteristics to restoration of riparian vegetation along rivers in arid south-western United States. Freshw. Biol. 52, 651–679.
Syvitski, J.P., Morehead, M.D., Bahr, D.B., Mulder, T., 2000. Estimating fluvial sediment transport: the rating parameters. Water Resour. Res. 36, 2747–2760.
Tananaev, N.I., 2013. Applying regression analysis to calculating suspended sediment runoff: specific features of the method. Water Res. 40, 585–592.
Thomas, R.B., 1988. Monitoring baseline suspended sediment in forested basins: the effects of sampling on suspended sediment rating curves. Hydrol. Sci. J. 33, 499–514.
Tóth, B., Bódis, E., 2015. Estimation of suspended loads in the Danube River at Göd (1668 river km), Hungary. J. Hydrol. 523, 139–146.
Vericat, D., Batalla, R.J., 2006. Sediment transport in a large impounded river: the lower Ebro, NE Iberian Peninsula. Geomorphology 79, 72–92.
Vörösmarty, C.J., et al., 2003. Anthropogenic sediment retention: major global impact from registered river impoundments. Glob. Planet. Chang. 39, 169–190.
Walling, D.E., 1974. Suspended sediment and solute yields from a small catchment prior to urbanization. In: Gregory, K.J., Walling, D.E. (Eds.), Fluvial Processes in Instrumented Watersheds. Institute of British Geographers.
Walling, D.E., 1977. Assessing the accuracy of suspended sediment rating curves for a small basin. Water Resour. Res. 13, 531–538.
Walling, D.E., Fang, D., 2003. Recent trends in the suspended sediment loads of the world's rivers. Glob. Planet. Chang. 39, 111–126.
Walling, D.E., Webb, B.W., 1988. The reliability of rating curve estimates of suspended sediment yield: some further comments. Sediment Budgets. 174, 337–349.
Wang, W.D., Zhao, Z.G., Rong, X.M., 2006. Analysis research on daily average sediment flux of suspended load in high-water period. J. Irrig. Drain. 25, 77–80.
Wang, X.D., Zhong, X.H., Liu, S.Z., Liu, J.G., Wang, Z.Y., Li, M.H., 2008. Regional assessment of environmental vulnerability in the Tibetan Plateau: development and application of a new method. J. Arid Environ. 72, 1929–1939.
Wen, A.B., Liu, S.Z., Fan, J.R., Zhu, P.Y., Zhou, L., Zhang, X.B., Zhang, Y.Y., Xu, J.Y., Bai, L.X., 2000. Soil erosion rate using ~(137)Cs technique in the middle Yalungtsangpo. J. Soil Water Conserv. (Chinese) 17, 47–50.
Wood, P.A., 1977. Controls of variation in suspended sediment concentration in the River Rother, West Sussex, England. Sedimentology 24, 437–445.
Wotling, G., Bouvier, C., 2002. Impact of urbanization on suspended sediment and organic matter fluxes from small catchments in Tahiti. Hydrol. Process. 16, 1745–1756.
Xu, K.Q., et al., 2005. Simulated sediment flux during 1998 big-flood of the Yangtze (Changjiang) River, China. J. Hydrol. 313, 221–233.
Yang, Z.G., Jian, J., Hong, J.C., 2014. Temporal and spatial distribution of extreme precipitation events in Tibet during 1961–2010. Plateau Meteorol. 33, 37–42 (Chinese).
Yao, T.D., Yao, Z.J., 2010. Impact of glacial retreat on runoff on Tibetan Plateau. Chin. J. Nat. 32, 4–8.
Zeng, C., Shao, M.A., Wang, Q.J., Zhang, J., 2011. Effects of land use on temporal-spatial variability of soil water and soil-water conservation. Acta Agr Scand B-S P. 61, 1–13.
Zhang, X.X., 2011. Spatial-temporal evolutional laws of the key hydrological elements in Yarlung Zangbo River Basin. Beijing Forestry University, Beijing (13–18 pp).